Geomechanics for Energy and the Environment 45 (2026) 100800

Contents lists available at ScienceDirect

Geomechanics for Energy and the Environment

journal homepage: www.elsevier.com/locate/gete

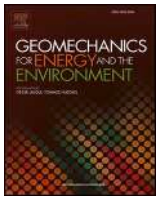

Finite element analysis of laterally loaded open-ended steel piles driven in chalk

Stavroula Kontoe [a,c], Giuseppe Pedone [b,*], Enrico Bellumat [b,a], Richard Jardine [c]

[a] Department of Civil Engineering, University of Patras, Aristotelous, Rio 26500, Greece
[b] Department of Civil, Environmental and Mechanical Engineering, University of Trento, Via Mesiano 77, Trento 38123, Italy
[c] Imperial College London, South Kensington Campus, London SW7 2AZ, United Kingdom

ARTICLE INFO

Editors-in-Chief: Prof A Ferrari

Key words:
Finite elements
Driven piles
Lateral loading
Chalk
Offshore wind energy

ABSTRACT

Open-ended steel piles are commonly driven to support offshore wind energy structures. Their design poses significant challenges in chalk, a very weak brittle limestone found in several regions worldwide. Impact driving causes chalk de-structuration and fracturing around the piles, greatly affecting their lateral load-bearing performance. This was observed in recent field tests undertaken in the UK on piles with different lengths, diameters and thicknesses, exhibiting both geotechnical and structural failures. Most of these lateral loading tests, including those conducted on larger and longer monopiles, were completed recently and were never analysed numerically. This paper presents results of 3D Finite Element analyses conducted on open-ended steel piles with different diameters (up to 1.22 m), embedded lengths (up to 10.16 m) and wall thicknesses (up to 44.5 mm), allowing to explore the marked scale effects observed on site. The newly available field tests also showed that steel yielding can occur before geotechnical failure is reached in chalk when testing piles with practical dimensions. However, steel yielding is usually neglected when modelling soil-pile interaction in geotechnical applications. The paper also aims at covering this gap by introducing a simplified modelling approach to account for elasto-plastic pile behaviour. The analyses delivered generally good matches with field behaviour and allowed to explore the main geotechnical uncertainties affecting accurate pile-chalk interaction predictions, mainly including the extent of the chalk fracturing induced by pile driving and its impact on chalk mechanical properties. The studies provide new and vital guidance for those involved in designing large driven piles for chalk sites.

1. Introduction

Large diameter open-ended steel tubular piles, which have long been adopted as common foundation solutions for port, bridge and other structures, are now being employed widely in offshore wind energy projects. The need to optimise the design of large numbers of offshore wind energy monopile structures, which sustain mainly lateral and moment loading, has led to intensive research, including the PISA (PIle Soil Analysis) Joint Industry Project (JIP).[1,2] PISA enabled more economical and reliable design for multiple projects involving monopiles (whose length-to-diameter ratios fall well below 10) by developing more accurate lateral analysis methods for sand and clay sites. However, PISA did not consider weak rocks, which are encountered increasingly frequently at potential development sites worldwide. One of the most common weak rocks in Northern Europe is chalk[3], which has caused severe difficulties in the design of offshore projects; see for example Barbosa et al.[4] or Carotenuto et al.[5]. Impact driving in low-to-medium density chalk de-structures the material close to pile shafts and induces additional fracturing in the surrounding rock, which strongly affect subsequent load-bearing behaviour; Muir Wood et al.[6], Buckley et al.[7]. Installation effects have been explored in model tests by Alvarez-Borges et al.[8] through X-ray computed tomography and investigated numerically using the Particle Finite Element Method (PFEM) by Previtali et al.[9]. However, the impact of chalk properties and installation effects on full scale service behaviour has yet to be explored systematically.

This paper aims to address this shortfall in current knowledge by considering the full suite of research pile tests conducted at Saint

* Corresponding author.
E-mail addresses: skontoe@upatras.gr (S. Kontoe), giuseppe.pedone@unitn.it (G. Pedone), enrico.bellumat@gruppotonet.com (E. Bellumat), r.jardine@imperial.ac.uk (R. Jardine).
[a] Present address: Tonet Group. Zona Industriale 6, 3203, Santa Giustina, Italy

https://doi.org/10.1016/j.gete.2026.100800
Received 19 November 2024; Received in revised form 24 November 2025; Accepted 3 February 2026
Available online 6 February 2026

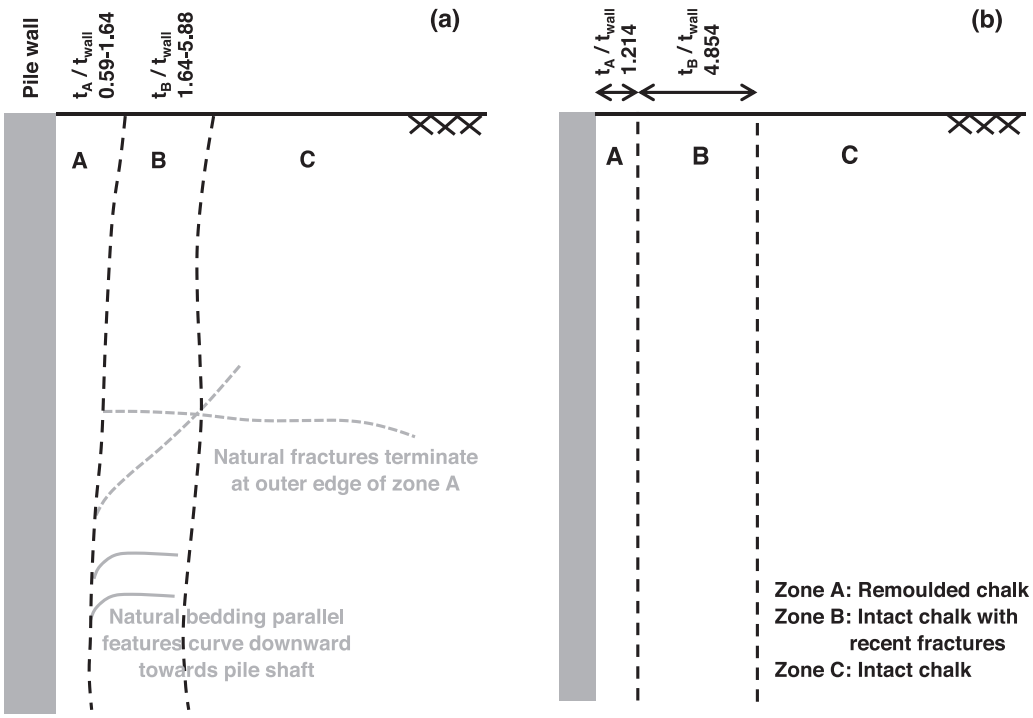

Fig. 1. Sketch of the chalk conditions next to the pile's shaft encountered by Buckley et al.7 (modified) during pile exhumation (a) and corresponding chalk zones considered in the 3D FE analyses by Pedone et al.1[9] (b).

Nicholas at Wade (SNW, Kent, UK) under the Windsupport Joint Industry Project (JIP) reported by Ciavaglia et al.[10], the Innovate UK JIP[7,11,12] and the comprehensive ALPACA (Axial and Lateral Pile Analysis in ChAlk) and ALPACA Plus JIPs[13–15]. The piles tested as part of these projects were all driven in low-to-medium density chalk (dry density, ρ_d=1.38–1.64 Mg/m^3) which classified as CIRIA grade B2/B3 following Lord et al.[16]. This grade signifies chalk discontinuities with 60-to-600 mm spacings and < 3 mm openings, that lead to mass hydraulic conductivities between 10^{-5} and 10^{-3} m/s. Extensive site characterisation studies demonstrated the SNW chalk's marked brittleness, with intact elements showing pronounced strain-softening in triaxial tests conducted under in-situ stresses; Vinck et al.[17]. Liu et al.[18] demonstrated that the chalk's behaviour is significantly pressure-dependent, transitioning from being brittle and dilative at low confining pressures to becoming ductile and contractive at confining pressures > 1 MPa.

Pedone et al.[19] undertook exploratory Finite Element (FE) analyses of two ALPACA JIP lateral loading tests on relatively short piles which involved a geotechnical failure mechanism, corresponding to a short free-headed pile failure mechanism according to Broms[20,21]. As such, their modelling approach did not consider elasto-plasticity for the steel forming piles, which were assumed, for simplicity, to behave purely elastic. Their modelling of the chalk's mechanical properties relied on the comprehensive field and laboratory characterisation campaigns reported by Vinck[22], Vinck et al.[17] and Liu et al.[18,23], which considered both intact and fully de-structured chalk. The damage induced by pile installation was accounted for indirectly by considering degraded mechanical properties in the chalk surrounding the pile. The different zones of damage around the piles were assigned on the basis of observations made by Buckley et al.[7] and summarised in Fig. 1a. Reliance was placed on earlier studies by Millar[24], Lord et al.[16] and Clayton et al.[25] when making key judgements regarding the mechanical properties of the damaged chalk.

The pilot lateral loading analysis by Pedone et al.[19] concentrated on a single pair of 0.508 m outer diameter (D) open-steel 'monopiles' with a wall thickness (t_w) of 20.6 mm, high yield stress steels and an embedded length (L) of 3.05 m (corresponding to L/D = 6). This analysis was able to capture the field response and the piles' purely geotechnical failure. However, the authors did not address whether their modelling strategy could scale to consider greater pile lengths, diameters, L/D ratios, steel grades or thicknesses accurately. This limited the confidence with which their methodology could be applied to, for example, help design offshore wind turbine monopiles, usually driven to several tens of metres depth and characterised by diameters up to several metres. The present paper aims to address this limitation by exploring whether the full set of field observed load-displacement, moment-rotation and bending moment-depth relationships could be captured through 3D FE analyses of laterally-loaded piles driven in chalk characterised by different diameters (up to 1.22 m), embedded lengths (up to 10.16 m) and pile wall thicknesses (up to 44.5 mm).

The lateral pile response is also heavily affected by steel yielding, typically neglected when modelling the behaviour of monopiles, not only with reference to chalk sites[19], but also when considering sand- or clay-dominated sites[26,27]. McAdam et al.[15] found, in the ALPACA field tests, that 0.508 m diameter piles with L/D ratios of 20, built in high yield stress X80 steel, and with a pile wall thickness t_w = 20.6 mm, underwent steel yielding significantly before reaching their ultimate 'failure', the latter associated with nominal lateral pile deflections of 10 %D at ground level. McAdam et al.[15] observed steel yielding before 'failure' also for a larger (1.22 m diameter) L/D = 6 ALPACA Plus pile built with standard (lower yield stress) steel and t_w = 24.6 mm. The present paper also aims at introducing a simplified modelling approach that allows to simulate steel yielding as part of routine soil-pile interaction FE analyses, demonstrating the significant impact that the proposed procedure might have when analysing the lateral pile behaviour up to large displacements.

The present study covers a range of pile geometries and failure mechanisms that have been fully explored for the first time by means of 3D FE analyses, providing previously unavailable guidance for chalk sites for those involved in designing driven piles under lateral loading. The paper outlines first the relevant lateral loading field test cases, before summarising the FE modelling approach adopted to simulate both chalk and pile behaviour (as well as their interaction). The

Table 1
Main features of the modelled piles.

	ALPACA		ALPACA Plus	Windsupport
	LD12-13	LD06-11	TP2	CP3
Outer diameter, D (m)	0.508	0.508	1.220	0.762
Embedded length, L (m)	3.050	10.160	7.320	4.000
Wall thickness, t_{wall} (mm)	20.6	20.6	24.6	44.5
L/D (-)	6	20	6	5.25
D/t_{wall} (-)	24.7	24.7	59.2	17.1
Load application level (m above ground level)	0.95–0.96	0.81–0.83	0.94	0.70
Material	X80 steel	X80 steel	S460 steel	API 5 L X65 steel

numerical simulations are then presented and discussed in relation to the field data. The outcomes allow important practical conclusions to be drawn regarding representative modelling and its potential pitfalls. Finally, research avenues are identified that should allow further refinement in predicting driven pile behaviour in chalk.

2. Pile tests

Table 1 summarises the pile test cases considered. These include the relatively rigid 'monopile' (L/D = 6) and relatively flexible (L/D = 20) 'friction' ALPACA tests on four 508 mm diameter piles made with high yield stress X80 steel. It also covers the ALPACA Plus 1220 mm diameter (L/D = 6) TP2 mild-steel 'monopile' described by McAdam et al.[15], and the L/D = 5.25, 762 mm diameter Test 3 mild-steel 'monopile' from the Windsupport programme[10], the latter referred to as CP3 herein. This suite considers far wider ranges of scales (L/D), pile wall thicknesses (t_w) and steel grades than those explored to date by means of numerical modelling[19]. Piles LD12/13, TP2, LD11/06 and CP3 required around 120, 165, 970 and 250 blows respectively, with a range of hammers to

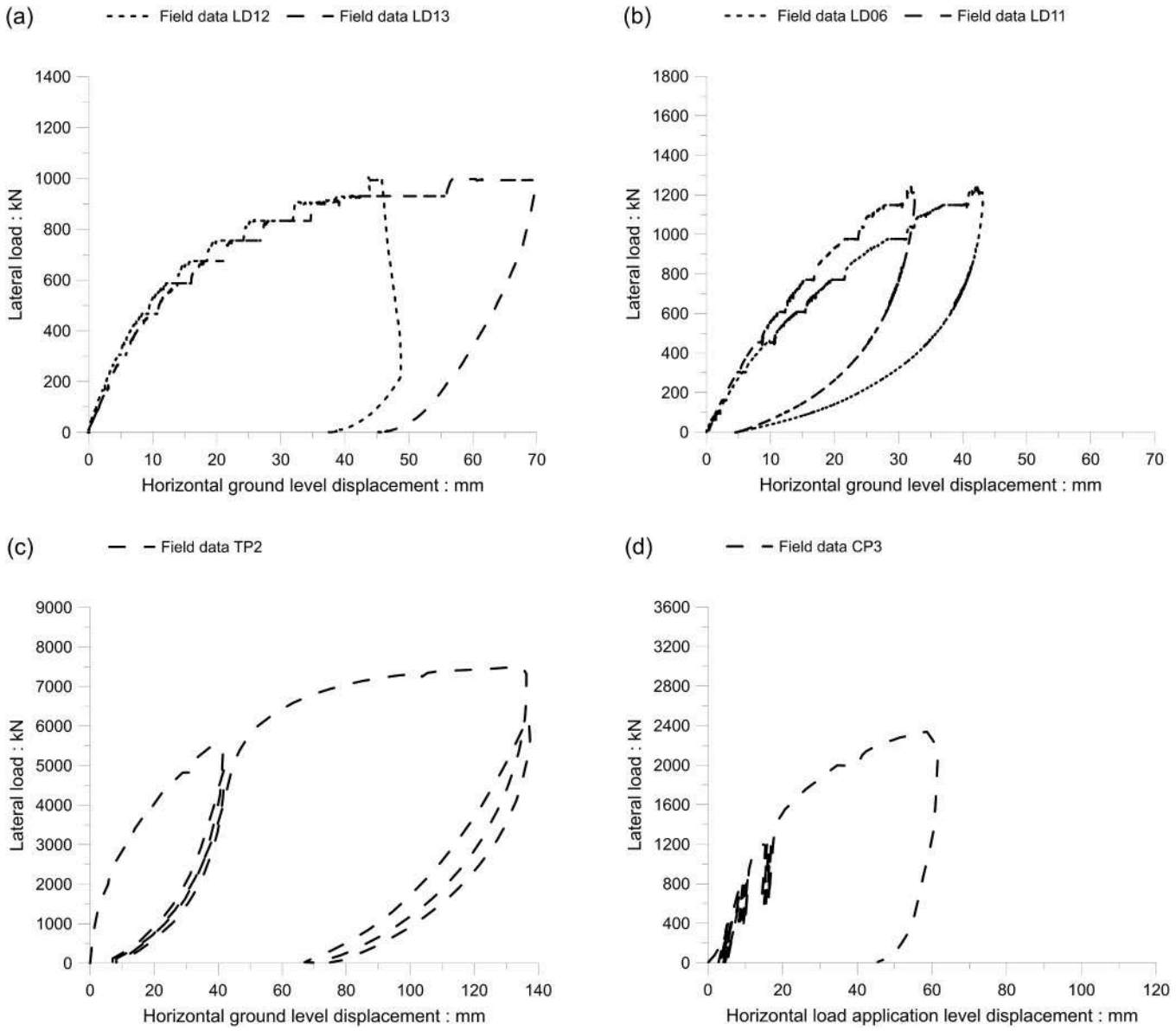

Fig. 2. Load-displacement curves: monitoring data for Piles LD12–13 (a), LD06–11 (b), TP2 (c) and CP3 (d) (monitoring data from McAdam et al.[15] and Ciavaglia et al.[10]).

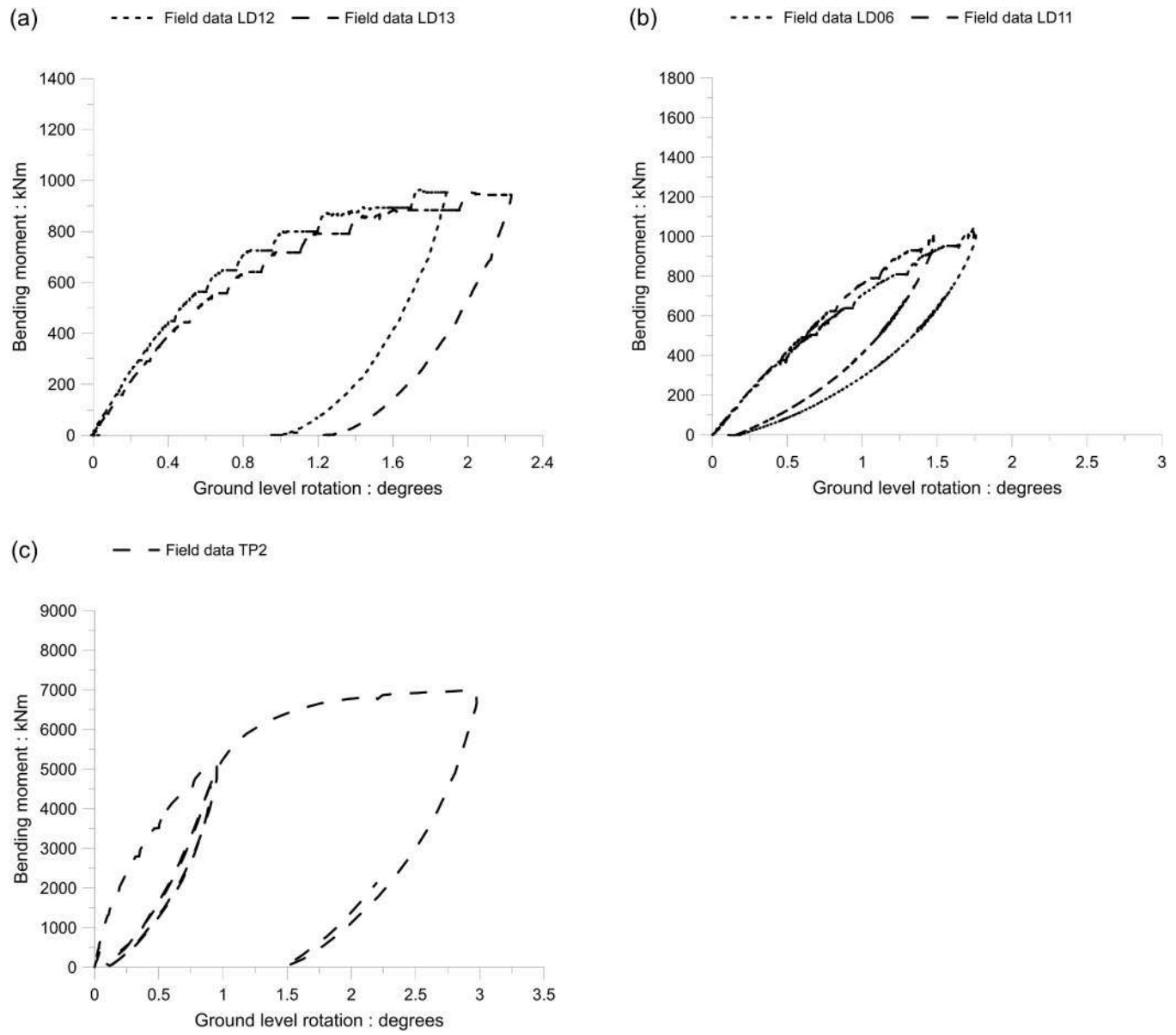

Fig. 3. Moment-rotation curves: monitoring data for Piles LD12–13 (a), LD06–11 (b) and TP2 (c) (monitoring data from McAdam et al.[5]).

reach their final depths. In comparison, the smaller piles whose zones of damage are illustrated in Fig. 1a (D = 139 mm, t_w = 8.5 mm), required around 100 blows to reach their final depths. The field lateral loading tests employed constant rate of loading stages separated by 'creep--pause' periods that continued until nominal 'failure', which is defined here as the point at which pile horizontal ground level (g.l.) displacements reached 10 %D. The lateral load-displacement and moment-rotation curves of all the piles considered in the present study (i.e. LD12–13, LD06–11, TP2, and CP3) are reported in Figs. 2 and 3, respectively.

Piles LD12–13 underwent purely geotechnical failure and were subsequently unloaded as shown in Figs. 2a and 3a. On the other hand, the higher L/D = 20 'friction' piles LD06 and LD11 were expected to experience a degree of structural plasticity and their loading was halted around the point of first steel yielding, as indicated in Figs. 2b and 3b. Pile TP2 was also unloaded just before yielding, which was expected to take place at a lateral load of around 5.7 MN, before it was re-loaded and taken to failure (see Figs. 2c and 3c). Windsupport's Pile CP3 was subjected initially to modest cyclic lateral loading, which probably affected its early load-displacement behaviour, before it was taken to monotonic failure (see Fig. 2d, in which, contrary to the other piles, horizontal displacements are not reported with reference to the g.l. but with reference to the load application level, i.e. 0.7 m above g.l.). Although moment-rotation data were available for piles LD12–13, LD06–11 and TP2[15], Ciavaglia et al.[10] do not report this information for pile CP3.

The ALPACA and ALPACA Plus piles had Fibre Bragg Grating (FBG) optical strain gauges strings bonded into shallow channels milled into their shafts that did not disrupt their cylindrical geometry. However, pile CP3's electrical resistance strain gauges were bonded to its outside and protected by substantial 90° steel channel sections welded to the shaft[10]. While these appurtenances probably stiffened the pile and altered its geometry during installation, their influence was uncertain and was not addressed in the present FE analyses.

3. Numerical modelling

3.1. Geometries and meshes

The 3D Finite Element (FE) analyses discussed in the paper were performed using PLAXIS 3D V24.1[28] employing a user defined

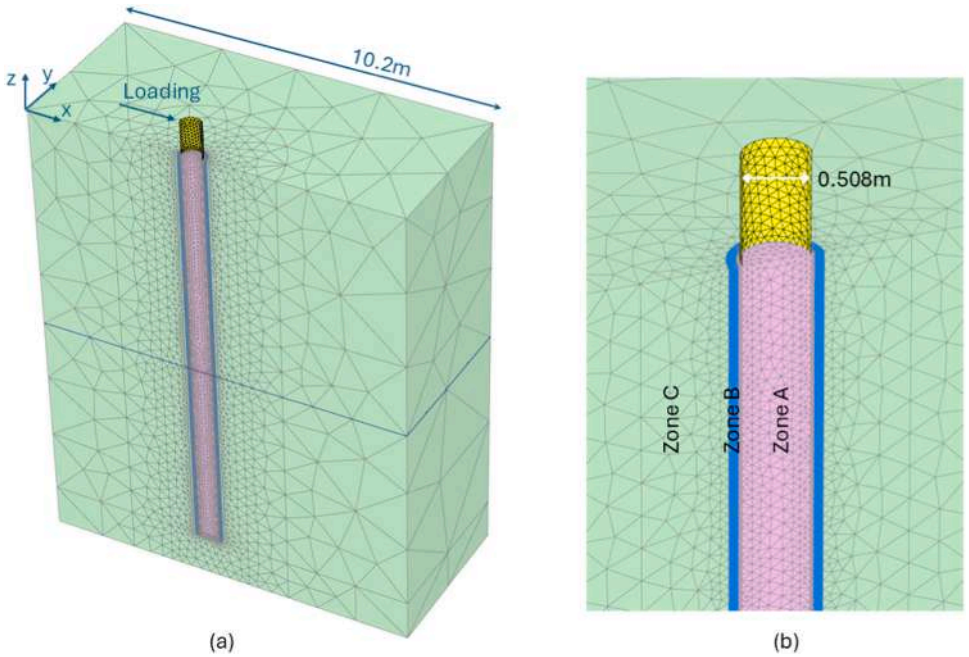

Fig. 4. Mesh generated for the 3D FE analysis of Piles LD06–11 (a) and details of the same mesh in the proximity of the pile (b).

constitutive model which incorporates both the pre-yield non-linear elastic behaviour[29] and a Mohr-Coulomb-type failure criterion[30,31]. The problem under investigation is symmetric, so only half-piles were modelled, as shown by the mesh generated for piles LD06–11 in Fig. 4a. Fig. 4b illustrates the details of the mesh in the proximity of the pile, where three different chalk regions have been considered, following the scheme identified by Buckley et al.[7] (Fig. 1a) and simplified by Pedone et al.[19] (Fig. 1b). The thicknesses t_A and t_B of the damaged Zones A and B were defined as multiples of the pile wall thickness, t_{wall}, according to Fig. 1a. It is worth highlighting that findings similar to those shown in Fig. 1a by Buckley et al.[7] were previously reported by Muir Wood et al.[6] and have been recently presented by Vinck et al.[32], confirming that the thickness of Zone A is comparable with the pile wall thickness. Assuming that the radial extents of the chalk affected by pile installation depends on wall thickness only, ratios of t_A/t_{wall}= 1.214 and t_B/t_{wall}= 4.854 were adopted in the main modelling sequence, following Pedone et al.[19]. However, it is recognised that the ratios t_A/t_{wall} and t_B/t_{wall} might vary between cases in the field due to local changes in chalk properties, pile geometries and/or installation details. It is also worth highlighting that, while the thickness of the fully de-structured Zone A was more easily identified on site after pile exhumation by water content measurements[7,32], identification of the Zone B thickness relied on visual observation of fracture intensity, which is more challenging to characterise precisely. In order to assess the impact of the t_B/t_{wall} value selected in the analyses, a parametric study was conducted and presented at the end of the paper.

The soil domain was discretised using 10-noded tetrahedral solid elements, while the pile was discretised using 6-noded plate elements (Fig. 4). 12-noded zero-thickness interface elements were also included around the outer and inner shafts of the pile, to allow for more representative simulations of the pile-chalk interaction. Among other things, interface elements are employed to accurately simulate pile-chalk interaction especially when active failure conditions are approached and gaps tend to form during lateral loading[15]. The meshes generated for the other piles employed different dimensions but shared the same general features as the LD06–11 case shown in Fig. 4.

3.2. Initial and boundary conditions

Due to the high mass permeability of the chalk at SNW, the lateral loading tests were all assumed to be fully drained. The displacement components were set to be zero at the bottom of the mesh, together with the displacement components orthogonal to the vertical boundaries. Pile loading was simulated by imposing horizontal (in the X direction) displacements at the experimental load application level (see Table 1 for load application elevations).

Initial effective stresses were defined based on laboratory and field data reported by Vinck et al.[17], i.e. by adopting: (i) an average bulk unit weight of 19.5 kN/m^3, (ii) a near-hydrostatic pore pressure distribution, and (iii) a coefficient of earth pressure at rest, K_0= 0.6 (that did not attempt to capture in detail the stress regime set up by pile installation, which is considered more extensively by Jardine et al.[13]). The water

Table 2
Main features of the pore pressure distributions adopted in the 3D FE analyses.

	ALPACA		ALPACA Plus	Windsupport
	LD12-13	LD06-11	TP2	CP3
Water table depth (m below ground level)	5.57	5.57	5.57	10
Pore pressure distribution below the water table	Linear and hydrostatic	Linear and hydrostatic	Linear and hydrostatic	Linear and hydrostatic
Pore pressure distribution above the water table	Linear and less than hydrostatic	Linear and less than hydrostatic	Linear and less than hydrostatic	Linear and less than hydrostatic
Pore water pressure at ground level (kPa)	-39.5	-39.5	-39.5	-70.9

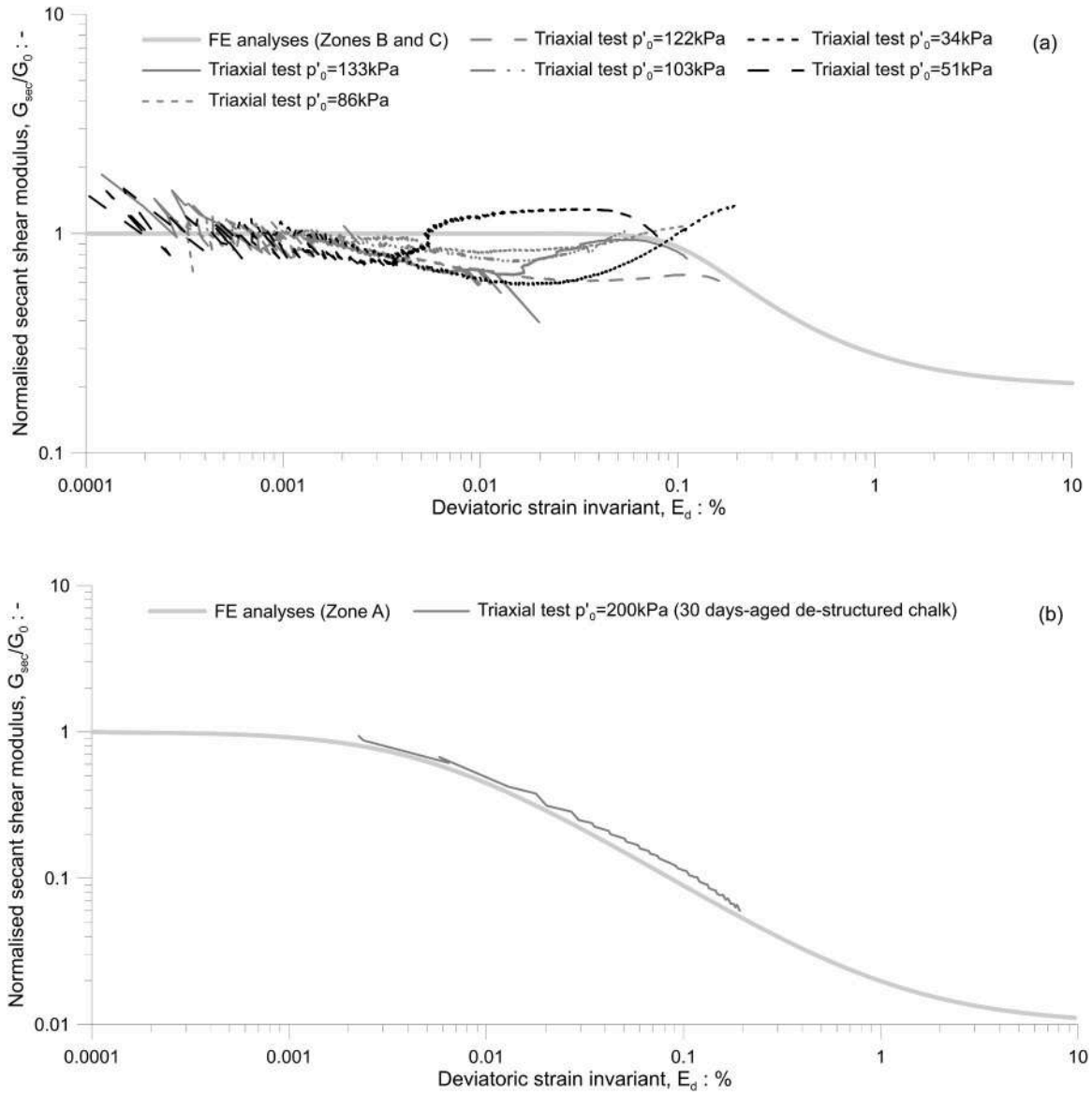

Fig. 5. Stiffness degradation curves adopted in the 3D FE analyses for fractured chalk in Zones B and C (a) and for fully de-structured chalk in Zone A (b) (modified after Pedone et al.1[9]; laboratory data from Vinck[22]).

table depths and pore pressure conditions in the different test areas are listed in Table 2[10,15].

3.3. Chalk mechanical properties

The main challenges associated with the simulation of chalk's mechanical behaviour relate to its fissured nature and potentially very brittle and pressure-dependent response. As discussed in Liu et al.[18], this brittleness becomes less pronounced as effective confining pressures exceed 1 MPa, with the chalk's dilative shearing behaviour gradually transforming to being ductile and contractive. Lateral pile loading generates maximum local mean effective stresses $p' > 2$ MPa at 'failure', making it essential to account for chalk's mechanical behaviour up to relatively high pressures when modelling its lateral loading field response[19].

Different constitutive models have been proposed in the literature to capture field behaviour of laterally-loaded piles driven in fractured chalk. The simplest model that gives adequate chalk-pile interaction predictions is a perfectly-plastic, non-linear elastic, Mohr-Coulomb model calibrated based on 'post-rupture' strength parameters[19], following experimental observations on fractured chalk made by Millar[24]. The 'post-rupture' strength parameters aimed to represent the broadly averaged response of fractured chalk, from small to large strains, from low to high confining pressures. The analyses described in the present paper were all conducted with this simple model and the constitutive parameters described in the following, according to the modelling approach introduced by Pedone et al.[19].

The post-rupture strength of SNW chalk over the relevant mean effective stress range is taken as matching an effective angle of shearing resistance, $\varphi' = 29°$, in combination with a cohesion $c' = 159$ kPa, as obtained post-peak from tests on intact chalk, conducted by Vinck et al.[17] and Liu et al.[18], that developed new fractures as they failed. Noting that both dilation and contraction are expected to occur within the chalk mass when moving from low to high confining pressures during pile lateral loading, the average dilation angle, ψ, was taken for simplicity as zero. The 'post-rupture' parameters were assumed to apply to the chalk mass within both Zone C, the naturally-fractured chalk, and Zone B, where additional fracturing had been induced by pile driving. The fully de-structured chalk in Zone A was simulated by adopting $\varphi' = 31.5°$, a nominal $c' = 3$ kPa and a dilation angle, $\psi = 0°$, following

Table 3
Chalk properties adopted in the 3D FE analyses.

Material	Model	G_0 (GPa)	G_{min} (GPa)	μ (-)	φ' (°)	c' (kPa)	ψ (°)
Naturally-fractured chalk (zone C)	Non-linear elastic perfectly-plastic Mohr-Coulomb	0.5	0.1	0.2	29.0	159	0
Recently-fractured chalk (zone B)	Non-linear elastic perfectly-plastic Mohr-Coulomb	0.05 *(*)*	0.01 *(*)*	0.2	29.0	159	0
De-structured chalk (zone A)	Non-linear elastic perfectly-plastic Mohr-Coulomb	1.0	0.01	0.2	31.5	3	0

(*) These stiffness values were varied as part of the parametric study presented in the paper

Wen et al.[33] and based on the triaxial tests on reconsolidated chalk 'putty' conducted by Vinck[22] on 30 day-aged samples. A nominal c' value different from zero was adopted for Zone A in order to minimise numerical instabilities.

The pre-yield chalk behaviour was simulated by adopting an isotropic non-linear elastic model[29–31] allowing for the degradation of the shear modulus, G, with the deviatoric strain invariant, E_d. Fig. 5 shows the stiffness degradation curves employed in the modelling, together with the laboratory data against which they were calibrated[17,22]. The maximum and the minimum shear moduli used in the analyses, G_0 and G_{min}, are listed in Table 3.

The maximum shear modulus selected for the naturally-fractured Zone C chalk, G_0= 0.5 GPa was based on field data[17]. Assessing the operational stiffness in the more fractured Zone B chalk was more challenging. Following evidence presented by Clayton et al.[25], its G_0 was assumed to be an order of magnitude lower (0.05 GPa) than in Zone C, while following the same stiffness degradation curve (as in Fig. 5a). Due to the uncertainties related to the Zone B stiffness characterisation, supplementary analyses aimed at assessing the impact of Zone B stiffness variations have been also conducted and presented towards the end of the paper. The G_0 and G_{min} values employed in the fully de-structured Zone A were found from locally instrumented triaxial tests by Vinck[22] on de-structured chalk samples that had been re-consolidated to appropriate stresses and allowed to age for 30 days before testing.

Considering the chalk retained within the piles, based on field observations and rational assumptions[7,13], the smaller diameter LD12–13 and LD06–11 cores (see Fig. 4) were considered as being fully de-structured (as in Zone A), while cores within the larger diameter CP3 and TP2 piles were sub-divided into Zones A, B and C materials.

3.4. Pile and pile-chalk interface mechanical properties

Piles LD12–13 and CP3 developed purely geotechnical failures, allowing isotropic linear elastic behaviour to be assumed in their steel walls, with Young's modulus E = 210 GPa and Poisson's ratio μ= 0.3. However, in order to better capture the interaction between piles and chalk, the plate elements forming the piles were generated by taking the outer pile diameter as the reference dimension (see Fig. 4b), while keeping the true (and significant) pile wall thickness in the plate elements (see Table 1). To avoid this approach overestimating the piles' bending stiffness E•J (where J is the pile section moment of inertia), the steel Young's modulus input into the FE analyses, E_{model}, was scaled down to achieve a match between modelled bending stiffness, E_{model}•J_{model}, and piles' true bending stiffness, E_{real}•J_{real}. A summary of the real and model pile properties is included in Table 4, indicating that Young's modulus reductions of < 20 % were required to simulate the real bending stiffness of the piles.

Table 4
Pile properties adopted in the 3D FE analyses.

	ALPACA		ALPACA Plus	Windsupport
	LD12-13	LD06-11	TP2	CP3
Model	Elastic	Elasto-plastic *(*)*	Elasto-plastic *(*)*	Elastic
Real pile outer diameter (m)	0.508	0.508	1.220	0.762
Real pile (intermediate) diameter (m)	0.487	0.487	1.195	0.718
Real pile wall thickness (mm)	20.6	20.6	24.6	44.5
Model pile (intermediate) diameter (m)	0.508	0.508	1.220	0.762
Model pile wall thickness (mm)	20.6	20.6	24.6	44.5
Real pile moment of inertia J_{real} (m^4)	$9.383 \bullet 10^{-4}$	$9.383 \bullet 10^{-4}$	$1.651 \bullet 10^{-2}$	$6.480 \bullet 10^{-3}$
Real Young's modulus E_{real} (GPa)	210.0	210.0	210.0	210.0
Model pile moment of inertia J_{model} (m^4)	$1.062 \bullet 10^{-3}$	$1.062 \bullet 10^{-3}$	$1.755 \bullet 10^{-2}$	$7.758 \bullet 10^{-3}$
Model Young's modulus E_{model} (GPa)	185.5	185.5	197.6	175.4
Poisson's ratio μ (-)	0.3	0.3	0.3	0.3
Plate element 'local' plastic modulus W_p (m^3/m)	N/A	$1.061 \bullet 10^{-4}$	$1.513 \bullet 10^{-4}$	N/A
Real yield stress, $\sigma_{y,real}$ (MPa)	N/A	550.0	460.0	N/A
Model yield stress, $\sigma_{y,model}$ (MPa)	N/A	505.6	441.5	N/A

(*) They were also modelled as purely elastic to investigate the impact of pile plasticity

A similar approach was adopted to model piles LD06–11 and TP2 (see Table 4), although for these cases the observed pile steel yielding was accounted for by adopting the relevant yield stress, σ_y, and the plastic section modulus, W_p, of the plate elements forming the pile. An elasto-plastic model was required to allow for the 'local' bending response of each plate element and, more importantly, for the 'global' bending response of the whole circular pile section. The model yield

Table 5
Pile-chalk interface properties adopted in the 3D FE analyses.

Material	Model	K_N (kN/m^3)	K_S (kN/m^3)	φ' (°)	c' (kPa)	ψ (°)
Pile-chalk interface	Linear elastic perfectly-plastic Mohr-Coulomb	$2.4 \bullet 10^6$	$3.0 \bullet 10^5$	34	1	0

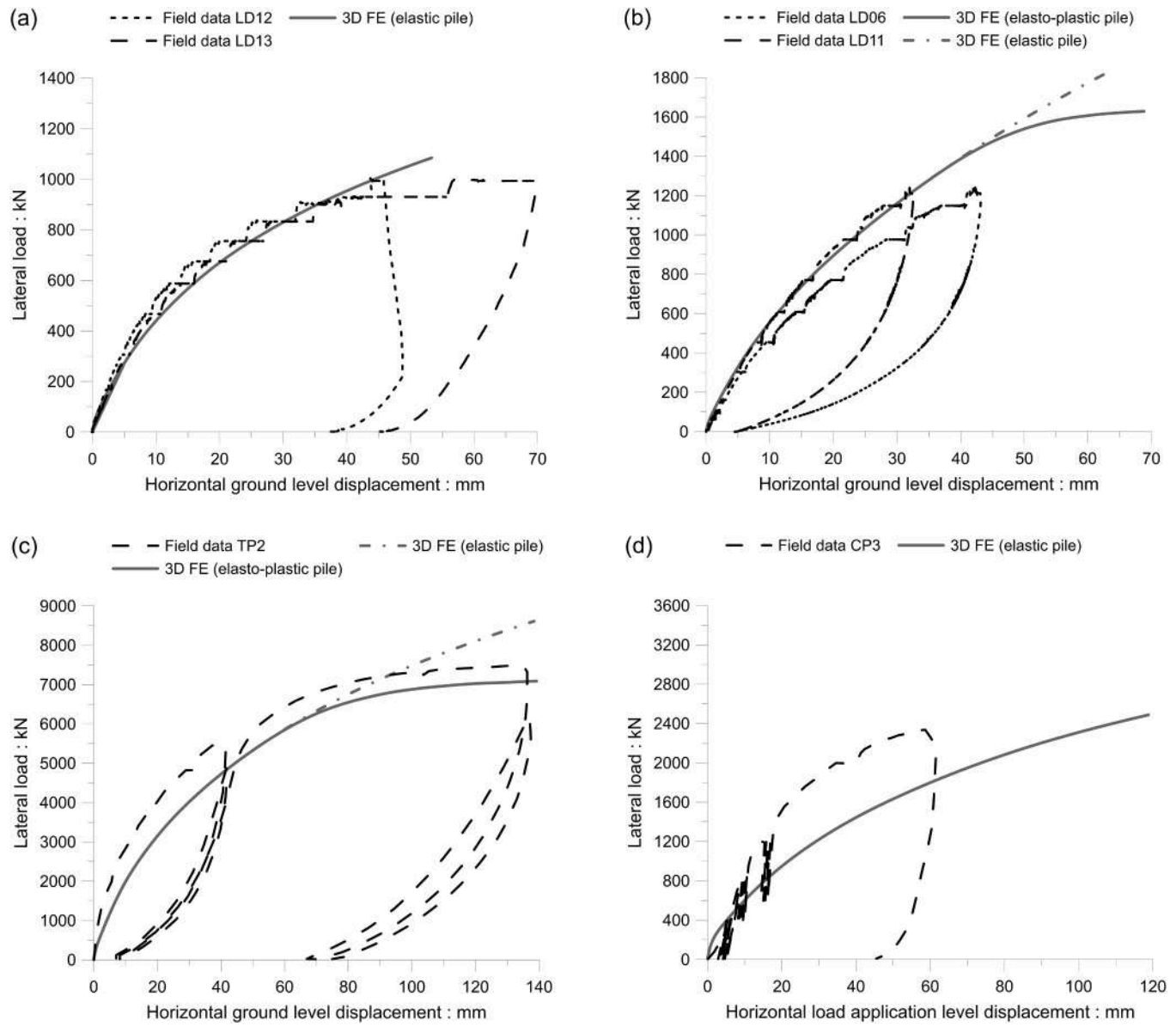

Fig. 6. Load-displacement curves: comparison between results of 3D FE analyses and monitoring data for Piles LD12–13 (a), LD06–11 (b), TP2 (c) and CP3 (d) (monitoring data from McAdam et al.[15], and Ciavaglia et al.[10]).

stresses, $\sigma_{y,model}$, were reduced with respect to the true values, $\sigma_{y,real}$, by < 10 % to match both yield and plastic moments, $M_{y,real}$ and $M_{p,real}$, of the LD06–11 and TP2 pile sections.

Zero-thickness interface elements were also introduced between the outer/inner surfaces of the plate elements simulating the piles and the solid elements simulating the chalk. The interface elements were assigned a linear-elastic perfectly-plastic Mohr-Coulomb model, adopted in combination with $\varphi' = 34°$, a nominal $c' = 1$ kPa and $\psi = 0°$, along with normal (K_N) and shear (K_S) stiffnesses of $2.4 \bullet 10^6$ kN/m^3 and $3 \bullet 10^5$ kN/m^3, respectively. These parameters, listed in Table 5, correspond to those adopted by Pedone et al.[19] and were identified through chalk-steel interface tests performed on suitably aged specimens by Vinck[22]. These laboratory tests allowed to identify the ultimate shear strength available at the chalk-steel interface, associated with $\varphi' = 34°$ for the steel types adopted as part of the ALPACA and the ALPACA Plus pile loading tests. The shear stiffness, K_S, available at the chalk-steel interface was also derived from the laboratory tests carried out by Vinck[22], while the normal stiffness, K_N, was defined following recommendations reported by Pedone et al.[34].

4. Results

4.1. Comparisons with the field measurements

The load-displacement, moment-rotation and moment-depth results from the main sequence of analyses are compared with the field test outcomes in Figs. 6, 7 and 8. By taking as a reference the more representative elasto-plastic pile behaviour for LD06–11 and TP2, it can be seen that generally good ultimate capacity (Fig. 6), moment-rotation response relationships (Fig. 7) and moment-depth profiles' matches (Fig. 8) were obtained with the field tests. The lateral load-displacement behaviour is also relatively well captured (Fig. 6), although (i) TP2's stiffness is slightly under-estimated, especially at low load levels (even though the corresponding moment-rotation response is well predicted), (ii) and the lateral displacements developed in test CP3 are more significantly under-predicted. Possible reasons for these discrepancies are discussed later. The finding that the ultimate lateral capacity is generally well predicted for all piles indicates that the post-peak strength properties obtained from intact chalk tests (as reported in

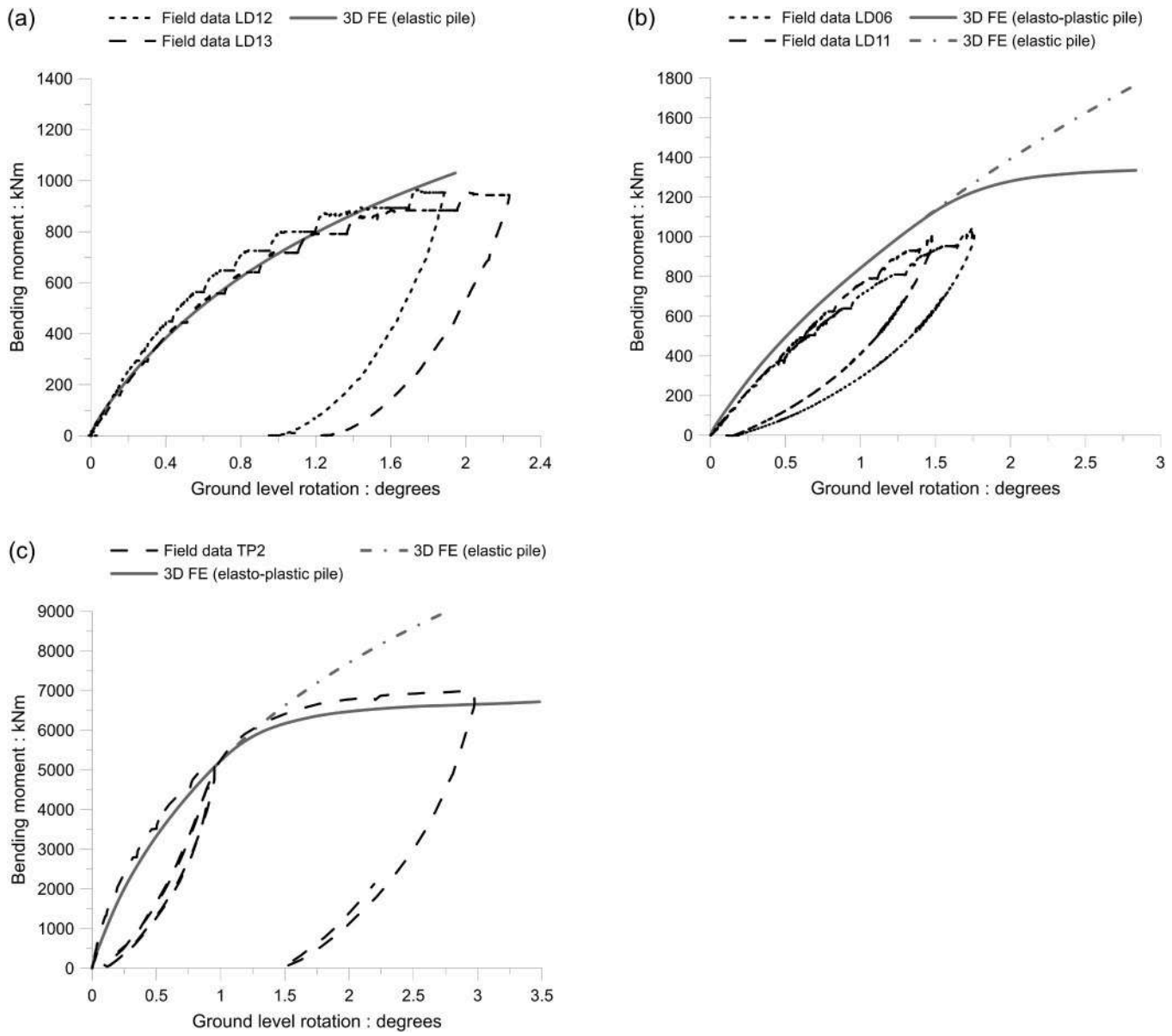

Fig. 7. Moment-rotation curves: comparison between results of 3D FE analyses and monitoring data for Piles LD12–13 (a), LD06–11 (b) and TP2 (c) (monitoring data from McAdam et al.1[5]).

Table 3) are broadly representative of the average mechanical behaviour of the fractured chalk as the piles approach failure.

4.2. *Impact of steel yielding on pile-chalk interaction*

Pile wall steel yielding was engaged during the tests conducted on piles LD06–11 and TP2. In order to explore the impact of pile plasticity, two modelling approaches were adopted for these cases that (i) accounted for yielding as described above (referred to as 'elasto-plastic' in Figs. 6 and 7) and (ii) assumed purely elastic behaviour in the piles (referred to as 'elastic' in Figs. 6 and 7). The results indicate overlapping predictions up to the point at which pile steel yielding is engaged. After this stage, the 'elasto-plastic' analyses predict a softer response for TP2 as it progresses to its ultimate lateral capacity, while the 'elastic' piles' load-displacement curves grow more markedly and exceeds the experimental observations (Figs. 6c and 7c). These results demonstrate the importance of accounting for pile plasticity in order to obtain accurate ultimate lateral pile capacity predictions, even for piles presenting relatively low L/D ratios like pile TP2, characterised by L/D = 6. Additional insights of the lateral response of this pile are presented in the following by looking at the deformed shape of the pile at failure, that shows the formation of a plastic hinge in the pile.

The formation of a plastic hinge was also observed for piles LD06–11 (Figs. 6b and 7b), even though the field tests were stopped soon after approaching the 1200 kN load, at which steel yielding was expected to start. For this reason, piles LD06–11 approached 20 and 40 mm horizontal g.l. displacements before the occurrence of any significant yield. Therefore, only one set of bending moment profile predictions are reported in Fig. 8 for these two key stages, taking as a main reference the analysis in which the elasto-plastic pile behaviour was modelled. It is worth highlighting that, at approximately 40 mm horizontal g.l. displacement, the 'elastic' and 'elasto-plastic' FE predictions start diverging (Fig. 6b), indicating the stage from which yielding starts propagating within the pile. At this stage, the FE analysis successfully indicates a maximum bending moment close to 2000 kNm at around 1 m below g.l. (Fig. 8d), a value extremely close to the yield moment of the pile section, $M_y = 2032$ kNm, the latter also measured on site at very similar depths.

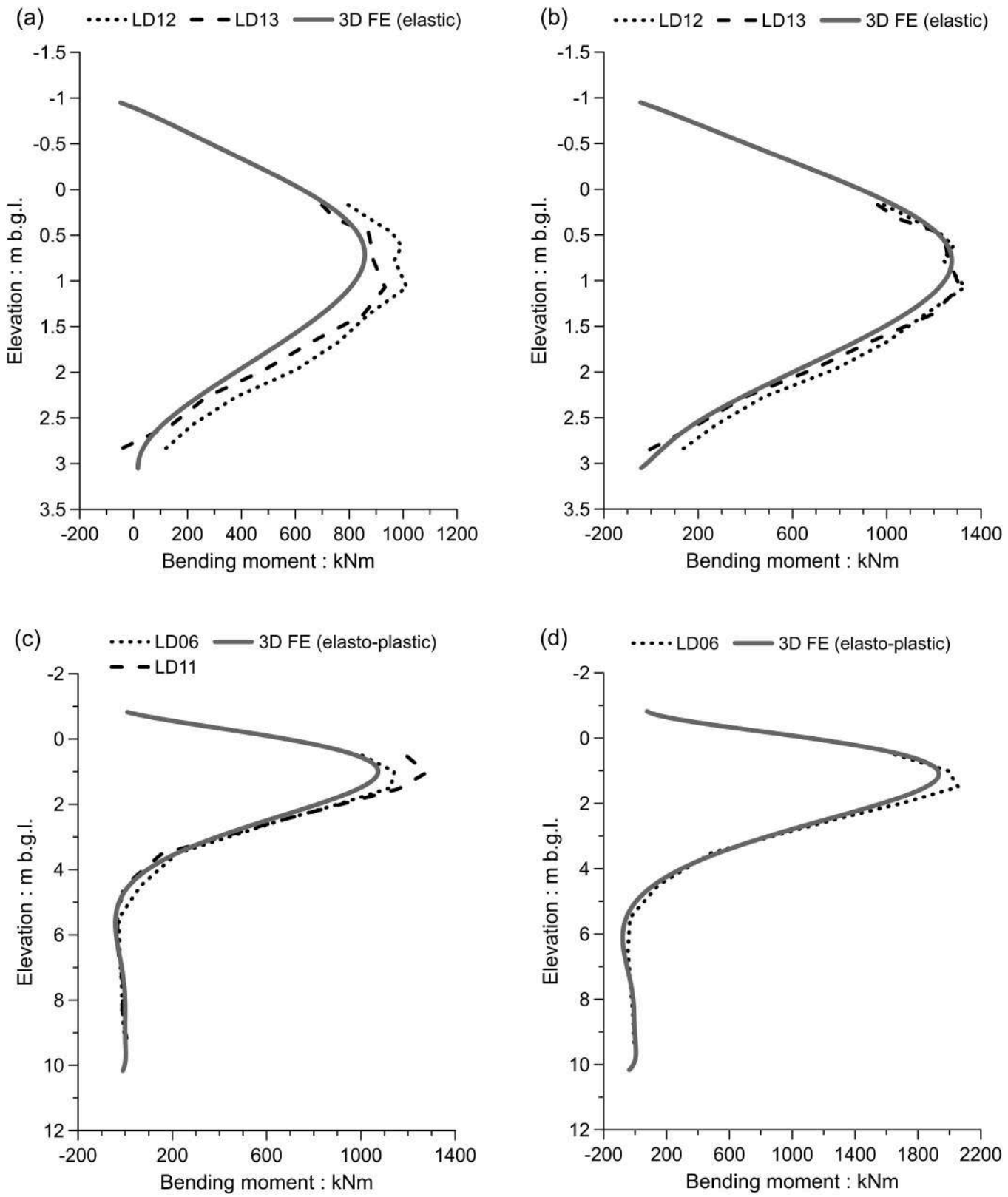

Fig. 8. Measured and predicted bending moment profiles at key stages of the LD12–13 and LD06–11 pile tests (a and b, 20 and 40 mm g.l. displacement for Piles LD12–13; c and d, 20 and 40 mm g.l. displacement for Piles LD06–11) (monitoring data from McAdam et al.[15]).

The predicted pile deformed shapes at failure, i.e. when 10 %D g.l. horizontal displacements were reached, are plotted in Fig. 9. The L/D = 20 piles LD06–11 (Fig. 9b) displayed a classical 'long-pile' failure mechanism[20,21] that incorporated structural pile failure, with gapping implied in the active region behind the pile head. Pile bending was evidently less important than rigid rotation for piles LD12–13 (Fig. 9a) and the relatively thick-walled pile CP3 (Fig. 9d), with L/D ratios of 6 and 5.25, respectively, which failed by nearly rigid rotation

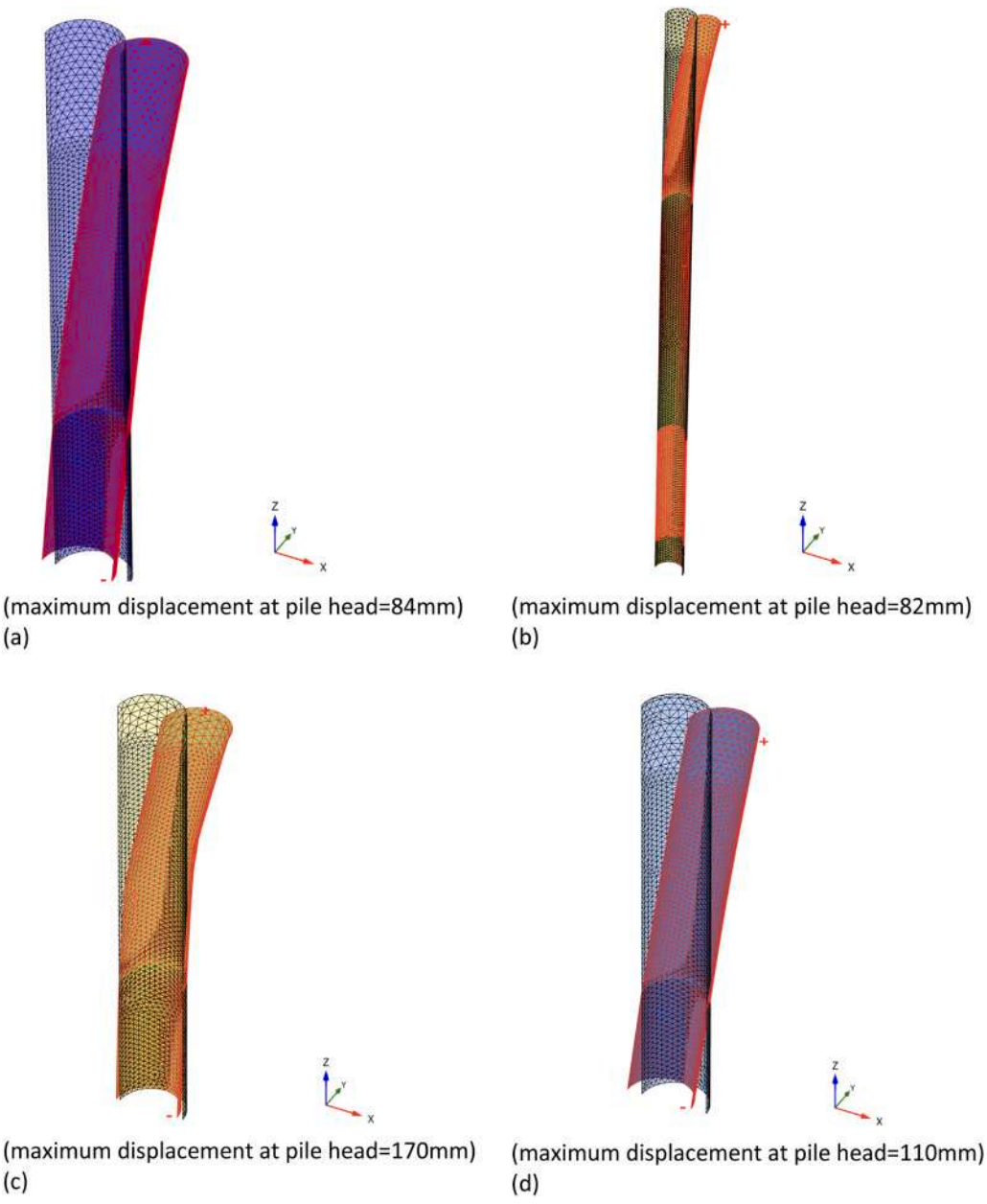

Fig. 9. Deformed shapes (scaled up 5 times) for Piles LD12–13 (a), LD06–11 (b), TP2 (c) and CP3 (d) at failure (corresponding to 10 %D horizontal g.l. displacement).

mechanisms, with rotation points roughly located at 2/3 of the embedded depths. However, as previously highlighted, Pile TP2 (Fig. 9c) showed the formation of a plastic hinge, despite its L/D ratio of 6, principally because of steel yielding of its relatively thin mild-steel walls. The gaps that form in the active regions behind the piles have a profound impact on the piles' unloading and cyclic loading responses[15].

Further insights are given by the p' and G/G_0 (stiffness decay) contour plots shown in Figs. 10 and 11, respectively, all referred to the 'failure' stage, as previously defined. Passive loading significantly increases the local p' to values that exceed 2 MPa in some locations as failure approaches (see Fig. 10), confirming the need for the chalk characterisation to include high-confining pressure laboratory tests. Even though most of the lateral ground deformation is developed within the most heavily loaded Zones A and B, a significant volume of the Zone C chalk is also taken into its non-linear range of stress-strain behaviour as loading levels rise (see Fig. 11). The volumes within which the 'failing' piles engage the chalk extend laterally by up to 3–4 diameters from the pile outer wall.

4.3. Parametric investigation on Zone B geometrical and mechanical features

While other aspects of the test on the 0.762 m diameter pile CP3 were estimated more satisfactorily, the predicted load-displacement curve fell well below the field trend (Fig. 6d). The lateral stiffnesses shown by the largest (1.22 m) diameter pile TP2 were also slightly under-predicted, especially over its early stages, but to a less marked degree. These outcomes suggest that the extents adopted for the damaged areas around these larger and thicker piles, and/or the stiffnesses assumed within them, were less representative than in the other cases. Parametric studies were undertaken to explore these questions further, with specific reference to the damaged Zone B, whose limited laboratory and field characterisation presents higher degrees of uncertainties.

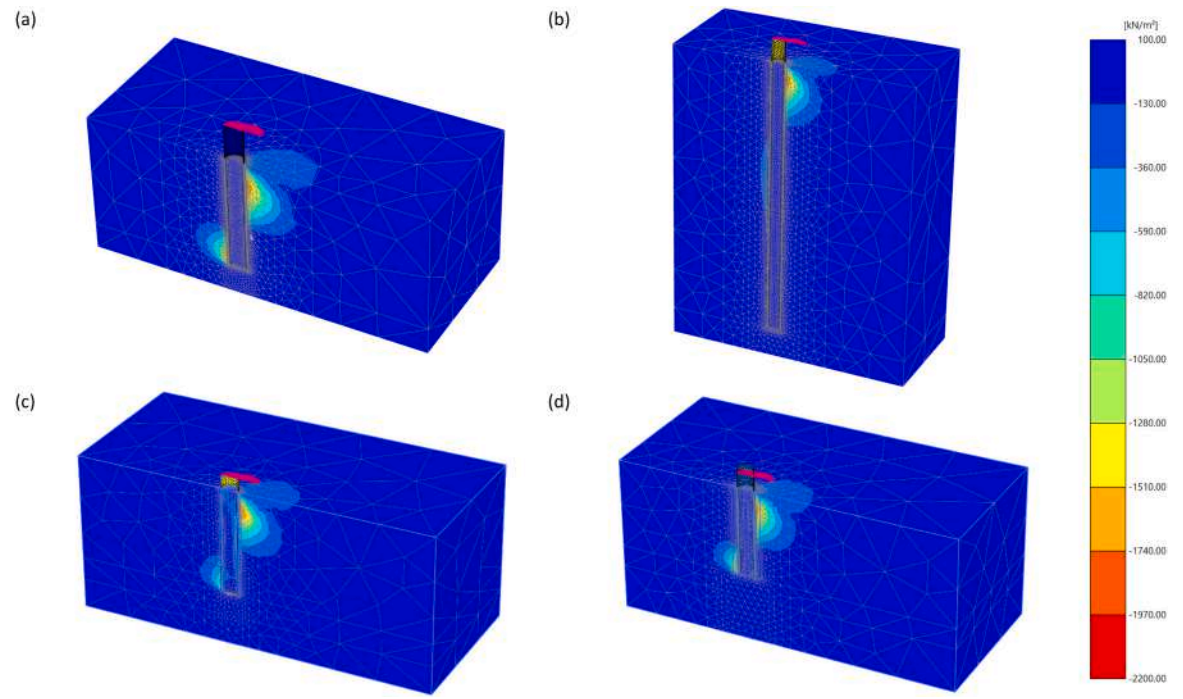

Fig. 10. Mean effective stress, p′, contours for Piles LD12–13 (a), LD06–11 (b), TP2 (c) and CP3 (d) at failure (corresponding to 10 %D horizontal g.l. displacement) (negative values indicate compression).

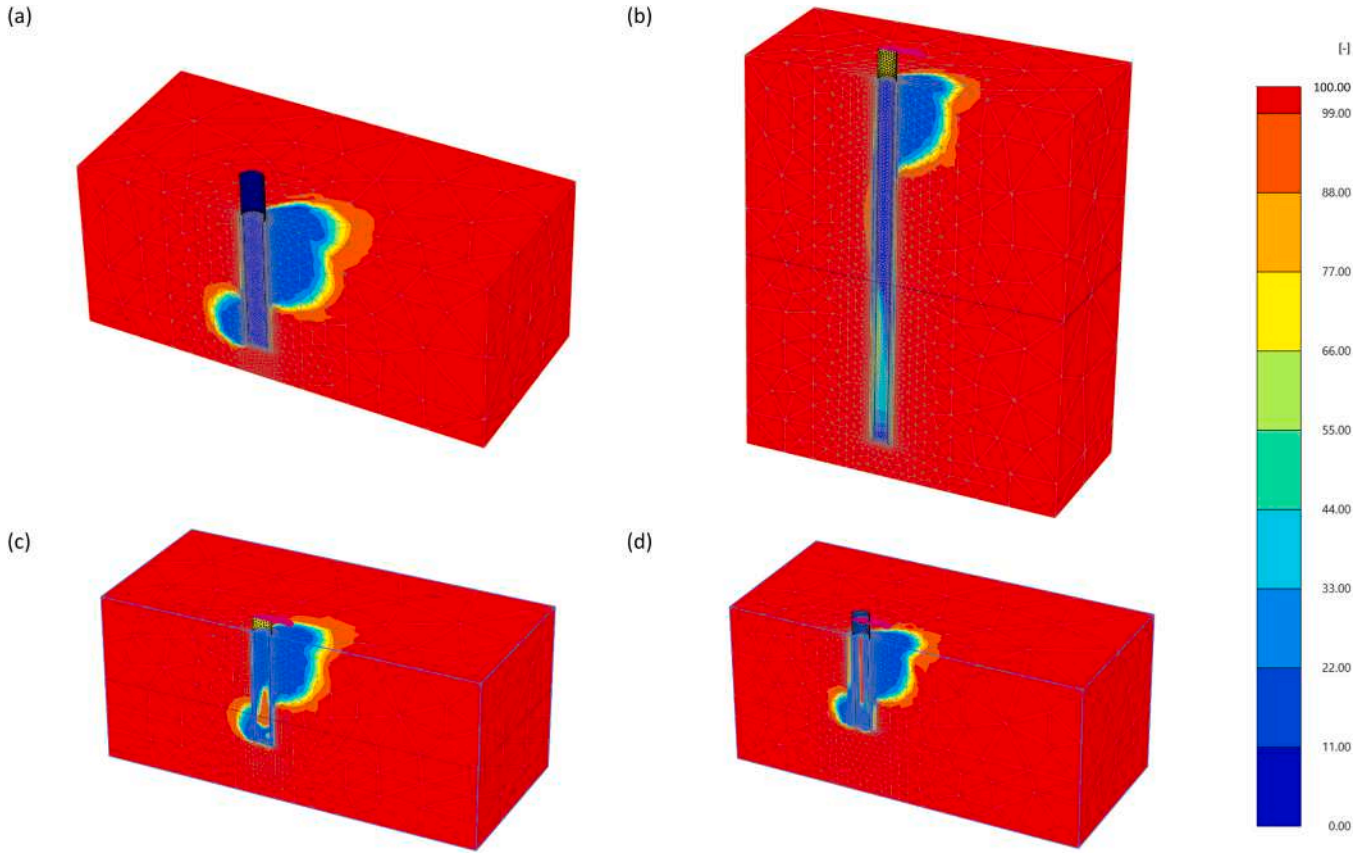

Fig. 11. Contours of G/G_0 for Piles LD12–13 (a), LD06–11 (b), TP2 (c) and CP3 (d) at failure (corresponding to 10 %D horizontal g.l. displacement).

4.3.1. Impact of Zone B stiffness

The least certain aspects of the chalk characterisation for the FE analyses were the assignment of appropriate stiffness values within Zone B, where most of the ground deformation occurs under lateral loading, and the radial extent of this additionally fractured region. Mismatches between the assumptions made and the field behaviour offer perhaps the

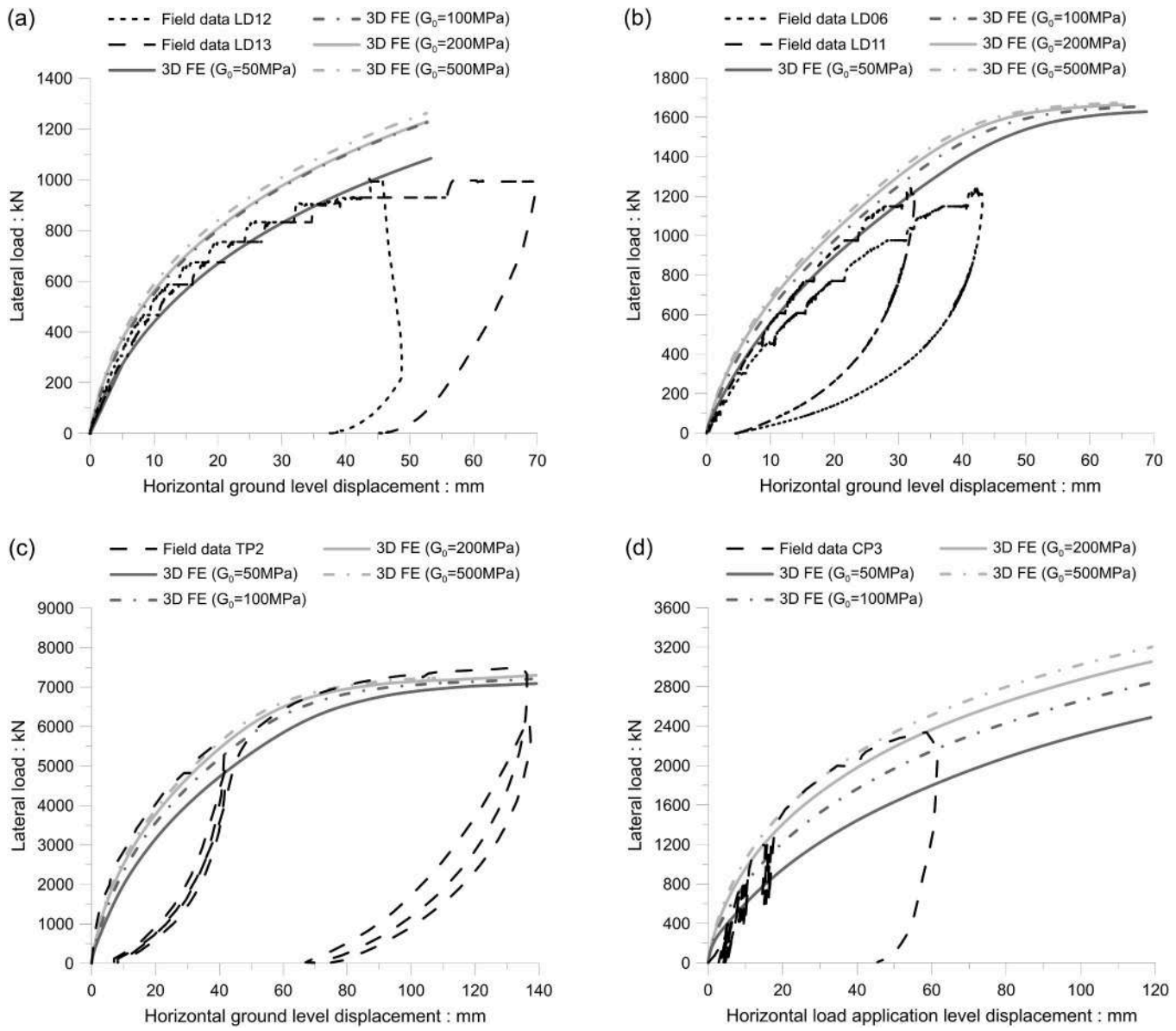

Fig. 12. Load-displacement curves: parametric study conducted on Piles LD12–13 (a), LD06–11 (b), TP2 (c) and CP3 (d) by varying the maximum stiffness (G_0) of Zone B (monitoring data from McAdam et al.[15], and Ciavaglia et al.[10]).

plausible cause of the FE analyses' under-prediction of pre-failure lateral displacements in the TP2 and CP3 tests.

To explore such uncertainties, a parametric investigation was undertaken into the influence of increasing stiffness in Zone B. The G_0 value was increased in three steps from 50 MPa up to 500 MPa (taking the Zone C value as a reasonable upper bound) while keeping the same stiffness degradation relationship (shown in Fig. 5a). It is worth noting that modelling Zone B with G_0= 500 MPa corresponds with a scenario in which Zone B is fully replaced by Zone C. The load-displacement and moment-rotation results of this parametric investigation are presented in Figs. 12 and 13, respectively. While increasing Zone B's G_0 stiffness led to notably better load-displacement agreement for test CP3 and an improvement for TP2, it led to over-predictions of the LD12–13 and LD06–11 piles' field lateral stiffnesses and capacities. The moment-rotation curves were already reasonably well estimated with the Zone B stiffness initially adopted, so its increase tended to induce, overall, field data over-estimations.

4.3.2. *Impact of Zone B thickness*

A second parametric study kept the initial G_0 value of 50 MPa for Zone B, but varied the Zone B thickness ratio within the $1.64 \leq t_B/t_{wall} \leq 5.88$ range reported by Buckley et al.[7], also indicated in Fig. 1a. This second study only considered piles CP3 and TP2, which had shown the largest load-displacement discrepancies and were the cases involving the thickest pile walls (24.6 mm and 44.5 mm). The results of this second parametric study are shown in Fig. 14 in terms of load-displacement curves. As expected, reducing the t_B/t_{wall} ratio led to greater lateral pile stiffness and capacity, although it was not possible to fully recover the field curve for pile CP3 within the range considered.

The numerical results suggest that further investigation is required into the extents of the damaged chalk Zone B and the field stiffness characteristics applying within it. However, with specific reference to pile CP3, it is postulated that the 90° angle steel strain gauge protection channels welded to the pile's outside shaft may have contributed to this pile's behaviour diverging far further from the FE predictions than the smoothly cylindrical ALPACA piles, including pile TP2. CP3's steel appurtenances may have changed the patterns of chalk damage inflicted

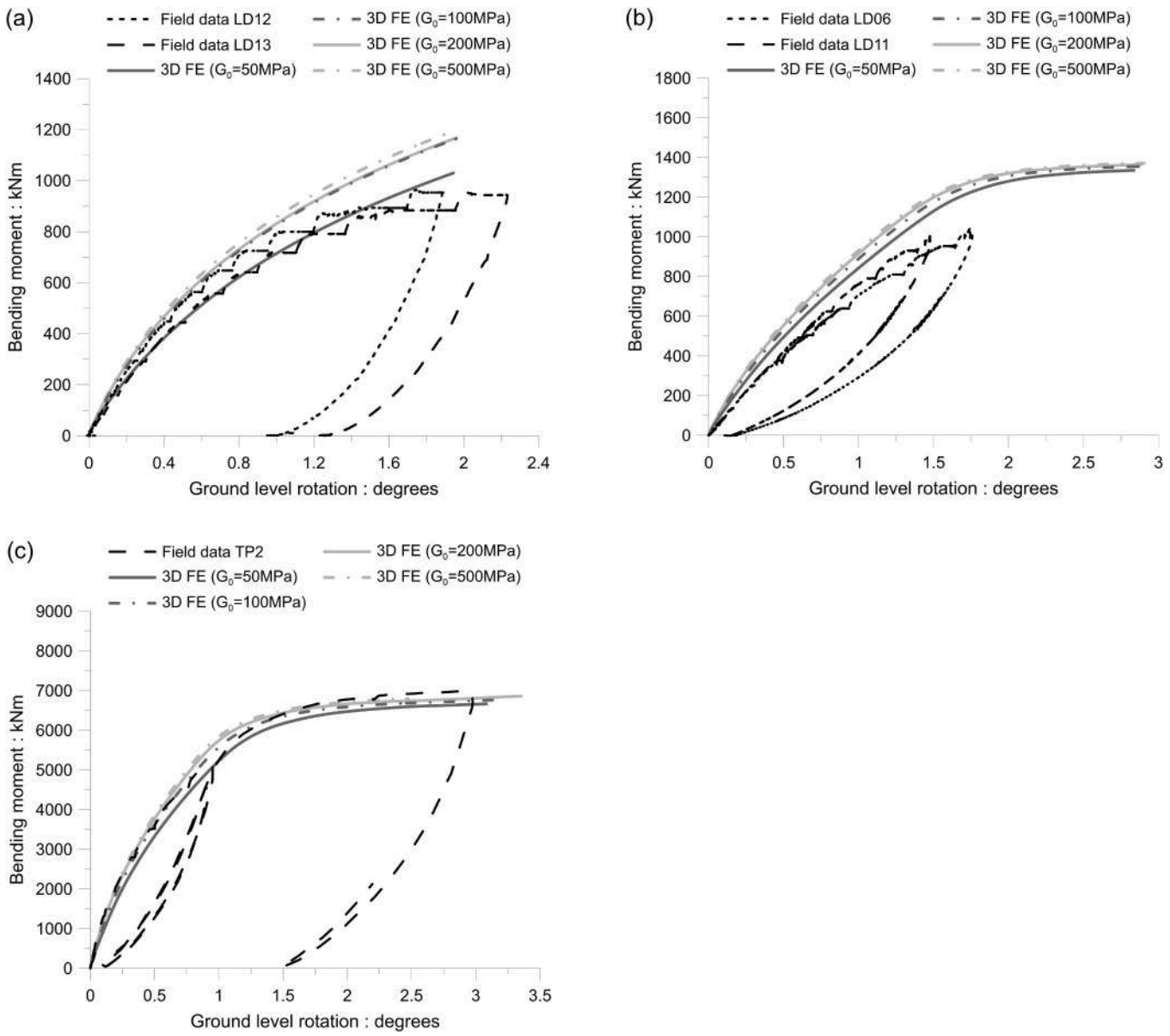

Fig. 13. Moment-rotation curves: parametric study conducted on Piles LD12–13 (a), LD06–11 (b) and TP2 (c) by varying the maximum stiffness (G_0) of Zone B (monitoring data from McAdam et al.1[5]).

around the shaft during driving, as well as adding to the pile's bending stiffness.

5. Summary and conclusions

The design of large open-steel piles to resist lateral loading for offshore wind-turbine monopiles and other structures poses significant challenges at chalk sites. Impact driving in low-to-medium density strata causes full de-structuration around the piles' shafts and induces additional fracturing in the surrounding rock, greatly affecting the piles' axial and lateral load-bearing performance. This paper reports generally successful 3D Finite Element (FE) lateral loading modelling of tests on strain-gauged, open-steel, driven piles with 0.508–1.22 m diameters, embedded lengths up to 10.16 m and a range of wall thicknesses extending up to 44.5 mm. The analyses captured the chalk properties identified from extensive in-situ and advanced laboratory testing, as well as installation effects. Potential yielding of the piles' steel walls, usually neglected when modelling soil-pile interactions in geotechnical applications, was also accounted for in the 3D FE analyses. The following conclusions can be drawn from the study:

1. The load-displacement, moment-rotation and bending moment profiles predicted for the spread of rigid to flexible ALPACA cases were generally satisfactory, especially when allowance was made for yielding in the pile steel. Ignoring pile yielding might cause severe ultimate lateral capacity overestimations, even for piles with relatively low L/D ratios.
2. The numerical analyses provide new insights into how lateral resistance develops around both rigid and flexible piles and the stresses they impose on the surrounding chalk mass. They also provide a design tool to help avoid steel yielding or excessive pile displacements developing in service.
3. Noting that the FE analyses presented in the paper generally predicted the ultimate piles' lateral capacities with reasonable accuracy, it appears that the 'post-rupture' strength properties obtained from triaxial tests on intact chalk provide representative estimates of the average shear strength applying in the fractured chalk at failure.

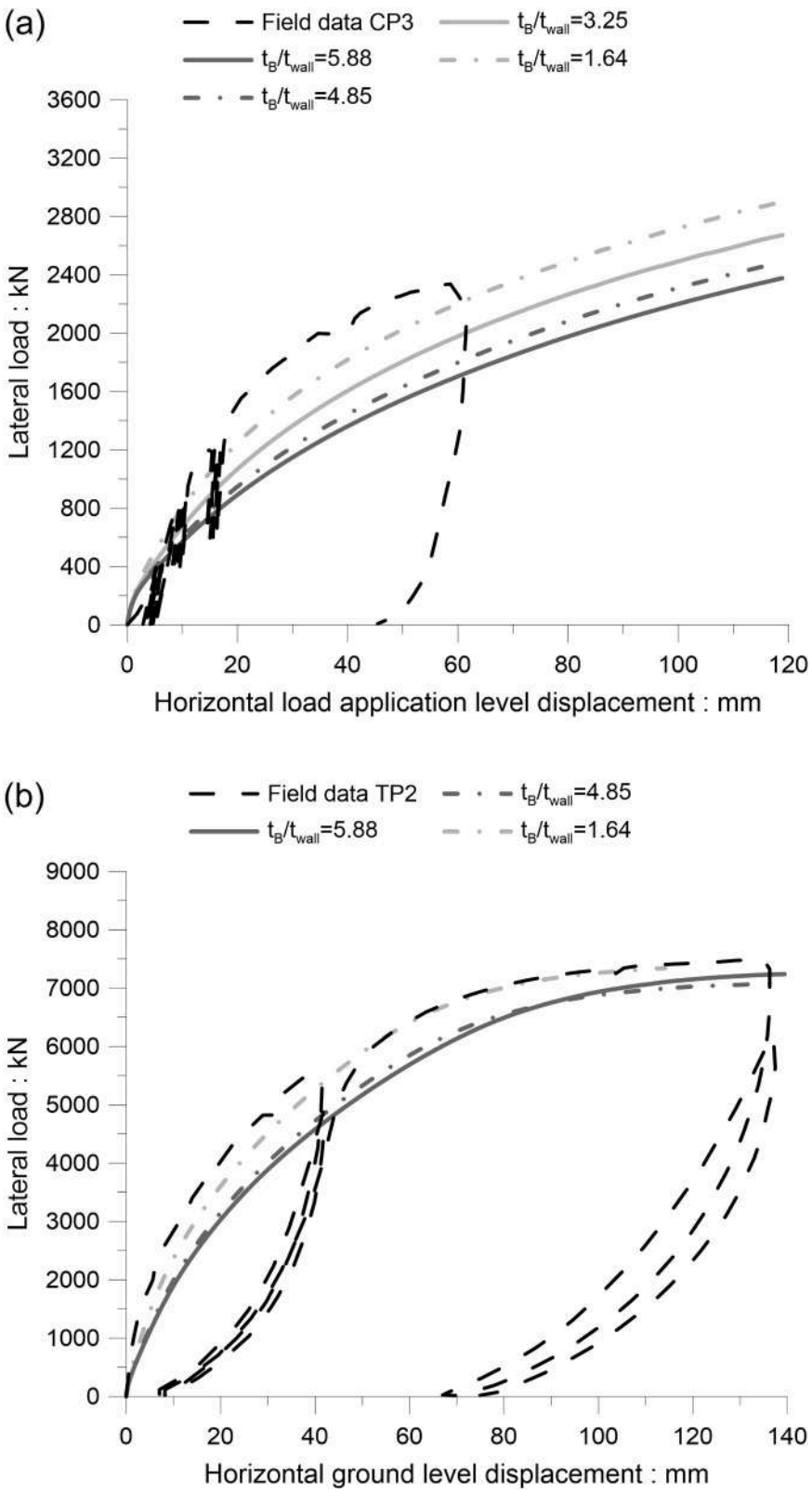

Fig. 14. Load-displacement curves: parametric study conducted on Piles CP3 (a) and TP2 (b) by varying the thickness of Zone B (monitoring data from Ciavaglia et al.1[0].

4. While the lateral load-displacement FE predictions were broadly representative of the field tests on piles with $24.7 \leq D/t_w \leq 59.2$, their predictions for the thicker walled ($D/t_w = 17.1$) Windsupport pile CP3 were less satisfactory. As the latter pile had experienced prior cyclic loading and carried steel strain gauge channels that may have altered its load-displacement behaviour, it appears that higher stiffnesses applied around this pile and/or that its damaged Zone B may have extended to smaller radial distances than assumed.

5. While the present results are encouraging for open piles with diameter-to-wall thickness ratios $D/t_w > 25$, the geotechnical characterisation of the de-structured and additionally fractured regions developed around open piles driven in chalk remain open to further, more detailed investigation. In particular, the results presented in the paper suggest that a more detailed Zone B mechanical characterisation is urgently needed for a better understanding of the interactions taking place between driven piles and chalk.
6. While highlighting the need for a more detailed characterisation of the chalk heavily affected by pile driving, the present paper allowed for a further validation of the modelling approach introduced by Pedone et al.[19]. Reliable representative numerical modelling of driven piles undergoing lateral loading is central to the PISA monopile design methodology[1,2], which is now applied widely by industry in multiple offshore windfarm projects. The work described in this paper provides the basis for applying the PISA approach to chalk-dominated formations, showing how 3D FE analyses may be undertaken to aid design for either specific monopile locations, or to develop 1D soil reaction curves by calibration from a sub-set of generically representative 3D FE analyses[26,27].

CRediT authorship contribution statement

Stavroula Kontoe: Writing – review & editing, Writing – original draft, Visualization, Validation, Supervision, Software, Resources, Methodology, Investigation, Formal analysis, Data curation, Conceptualization. **Giuseppe Pedone:** Writing – review & editing, Writing – original draft, Visualization, Validation, Supervision, Resources, Project administration, Methodology, Investigation, Funding acquisition, Data curation, Conceptualization. **Enrico Bellumat:** Writing – review & editing, Visualization, Validation, Methodology, Investigation, Formal analysis, Data curation. **Richard Jardine:** Writing – review & editing, Writing – original draft, Methodology, Investigation, Conceptualization.

Declaration of Competing Interest

The authors declare that they have no known competing financial interests or personal relationships that could have appeared to influence the work reported in this paper.

Acknowledgements

The authors express their gratitude to colleagues at their Universities and the grant donors and sponsors in the ALPACA and ALPACA Plus projects. They also thank Dr Ross McAdam and Prof Andrea Diambra for their help with details of the ALPACA and Windsupport field tests, and Trento University for Bellumat's support through Pedone's grant No. 40202493.

Data availability

Data will be made available on request.

References

1. Burd HJ, Taborda DMG, Zdravković L, et al. PISA design model for monopiles for offshore wind turbines: application to a marine sand. *Géotechnique*. 2020;70(11): 1048–1066. https://doi.org/10.1680/jgeot.18.P.277.
2. Byrne BW, Houlsby GT, Burd HJ, et al. PISA design model for monopiles for offshore wind turbines: application to a stiff glacial clay till. *Géotechnique*. 2020;70(11): 1030–1047. https://doi.org/10.1680/jgeot.18.P.255.
3. Mortimore RN. The 11th glossop lecture: making sense of chalk: a total-rock approach to its engineering geology. *Q J Eng Geol Hydrogeol*. 2012;45(3):252–334. https://doi.org/10.1144/1470-9236/11-052.
4. Barbosa P., Geduhn M., Jardine R.J., Schroeder F.C.Large scale offshore static pile tests – practicality and benefits. In: Proc. 8th International Conference on Offshore Site Investigation and Geotechnics. London, UK. 12-14 September 2017, p. 644-651. doi.org/10.3723/OSIG17.644.
5. Carotenuto P, Meyer VM, Strøm PJ, Cabarkapa Z, John St, Jardine H. RJ. Installation and axial capacity of the Sheringham Shoal offshore wind farm monopiles – a case history, 17-18. In: Lawrence JA, Preene M, Lawrence UL, Buckley RM, eds. *Engineering in Chalk: Conference Proc*. London, UK: Institution of Civil Engineers (ICE) Publishing; September 2018:117–122. https://doi.org/10.1680/eiccf.64072.117, 17-18.
6. Muir Wood A, Mackenzie B, Burbury D, et al. Design of large diameter monopiles in chalk at westermost rough offshore wind farm, 12-15. In: Meyer V, ed. Oslo, Norway: Taylor & Francis Books Ltd; June 2015:723–728. Proc. 3rd International Symposium on Frontiers in Offshore Geotechnic; 1.
7. Buckley RM, Jardine RJ, Kontoe S, Parker D, Schroeder FC. Ageing and cyclic behaviour of axially loaded piles driven in chalk. *Géotechnique*. 2018;68(2): 146–161. https://doi.org/10.1680/jgeot.17.P.012.
8. Alvarez-Borges FJ, Ahmed S, Madhusudhan BN, Richards DJ. Investigation of pile penetration in calcareous soft rock using X-ray computed tomography. *Int J Phys Model Geotech*. 2021;22(1):38–52. https://doi.org/10.1680/jphmg.20.00031.
9. Previtali M., Ciantia M.O., Riccio T.Numerical installation of OE piles in soft rocks within the GPFEM framework. In: Zdravković L., Konte S., Taborda D.M.G., Tsiampousi A., eds. In: Proc. 10th European Conference on Numerical Methods in Geotechnical Engineering. London, UK. 26-28 June 2023. doi.org/10.53243/NUMGE2023-322.
10. Ciavaglia F, Carey J, Diambra A. Monotonic and cyclic lateral tests on driven piles in Chalk. *Proc Inst Civ Eng (ICE) Geotech Eng*. 2017;170(4):353–366. https://doi.org/10.1680/jgeen.16.00113.
11. Buckley RM, Jardine RJ, Kontoe S, Lehane BM. Effective stress regime around a jacked steel pile during installation ageing and load testing in chalk. *Can Geotech J*. 2018;55(11):1577–1591. https://doi.org/10.1139/cgj-2017-0145.
12. Buckley RM, Jardine RJ, Kontoe S, Barbosa P, Schroeder FC. Full-scale observations of dynamic and static axial responses of offshore piles driven in chalk and tills. *Géotechnique*. 2020;70(8):657–681. https://doi.org/10.1680/jgeot.19.TI.001.
13. Jardine RJ, Buckley RM, Liu T, et al. The axial behaviour of piles driven in chalk. *Géotechnique*. 2024;74(6):553–569. https://doi.org/10.1680/jgeot.22.00041.
14. Jardine R.J., Buckley R.M., Liu T., Driven pile behaviour in low-to-medium density chalk: the ALPACA JIP outcomes. Innovative Geotechnologies for Energy Transition: In: Proc. 9th International Conference on Offshore Site Investigations and Geotechnics. SUT, London, UK. 12-14 September 2023. doi.org/10.3723/QMFP7598.
15. McAdam RA, Buckley RM, Schranz F, et al. Monotonic and cyclic lateral loading of piles in low to medium density chalk. *Géotechnique*. 2024. https://doi.org/10.1680/jgeot.23.00484.
16. Lord JA, Clayton CRL, Mortimore RN. *Report C574: Engineering in Chalk*. London, UK: Construction Industry Research and Information Association (CIRIA); 2002.
17. Vinck K, Liu T, Jardine RJ, et al. Advanced in-situ and laboratory characterisation of the ALPACA chalk research site. *Géotechnique*. 2024;74(6):512–526. https://doi.org/10.1680/jgeot.21.00197.
18. Liu T, Ferreira PMV, Vinck K, Coop MR, Jardine RJ, Kontoe S. The behaviour of a low- to medium- density chalk under a wide range of pressure conditions. *Soils Found*. 2023;63(1), 101268. https://doi.org/10.1016/j.sandf.2022.101268.
19. Pedone G, Kontoe S, Zdravković L, Jardine R, Vinck K, Liu T. Numerical modelling of laterally loaded piles driven in low-to-medium density fractured chalk. *Comput Geotech*. 2023;156, 105252. https://doi.org/10.1016/j.compgeo.2023.105252.
20. Broms BB. Lateral resistance of piles in cohesive soils. *J Soil Mech Found Div (ASCE)*. 1964;90(2):27–64. https://doi.org/10.1061/JSFEAQ.0000611.
21. Broms BB. Lateral resistance of piles in cohesionless soils. *J Soil Mech Found Div (ASCE)*. 1964;90(3):123–156. https://doi.org/10.1061/JSFEAQ.0000614.
22. Vinck K. *Advanced Geotechnical Characterisation to Support Driven Pile Design at Chalk Sites*. London, UK: PhD thesis, Imperial College; 2021.
23. Liu T, Ahmadi-Naghadeh R, Vinck K, et al. An experimental investigation into the behaviour of de-structured chalk under cyclic loading. *Géotechnique*. 2024;74(6): 540–552. https://doi.org/10.1680/jgeot.21.00199.
24. Millar MJ. *The Stress-strain Behaviour of Jointed Chalk*. UK: PhD thesis, University of Brighton; 2000.
25. Clayton CRL, Matthews MC, Heymann G. The chalk, 2-4. In: Tan TS, Phoon KK, Hight DW, Leroueil S, eds. Proc. 1st International Workshop on Characterisation and Engineering Properties of Natural Soils. Singapore. 1.
26. Taborda DMG, Zdravković L, Potts DM, et al. Finite element modelling of laterally loaded piles in a dense marine sand at Dunkirk. *Géotechnique*. 2020;70(11): 1014–1029. https://doi.org/10.1680/jgeot.18.PISA.006.
27. Zdravković L, Taborda DMG, Potts DM, et al. Finite-element modelling of laterally loaded piles in a stiff glacial clay till at Cowden. *Géotechnique*. 2020;70(11): 999–1013. https://doi.org/10.1680/jgeot.18.PISA.005.
28. Bentley Systems, 2024. PLAXIS 3D 2024.1: 2 - Reference Manual.
29. Taborda DMG, Potts DM, Zdravković L. On the assessment of energy dissipated through hysteresis in finite element analysis. *Comput Geotech*. 2016;71:180–194. https://doi.org/10.1016/j.compgeo.2015.09.001.
30. Taborda D.M.G., Kontoe S., Tsiampousi A. IC MAGE Model 01 – strain hardening/softening Mohr-Coulomb failure criterion with isotropic small strain stiffness. Version 1.7. Zenodo; 2022. doi:10.5281/zenodo.7198927.
31. Taborda D.M.G., Kontoe S., Tsiampousi A. 2022b. IC MAGE UMIP – universal model interface for PLAXIS. Version 3.2. Zenodo; 2022. doi: 10.5281/zenodo.7129726.
32. Vinck K., Liu T., Jardine R., Lawrence J., Buckley R.Characterising the damage developed around piles by percussive driving in low-to-medium density chalk. In. Abadie C., Li Z., Blanc M., Thorel L., eds. In: Proc. 5th International Symposium on

Frontiers in Offshore Geotechnic. Nantes, France. 9-13 June 2025. doi.org/10.53243/ISFOG2025-608.
33. Wen K, Kontoe S, Jardine R, Liu T. Finite element modelling of pipe piles driven in low-to-medium density chalk under monotonic axial loading. *Comput Geotech*. 2024; 172, 106458. https://doi.org/10.1016/j.compgeo.2024.106458.
34. Pedone G., Kontoe S., Zdravković L., Jardine R., Potts D.A sensitivity study on the mechanical properties of interface elements adopted in finite element analyses to simulate the interaction between soil and laterally loaded piles. In: Zdravković L., Konte S., Taborda D.M.G., Tsiampousi A., eds. Proc. 10th European Conference on Numerical Methods in Geotechnical Engineering. London, UK. 26-28 June 2023. doi.org/10.53243/NUMGE2023-148.